Characterization of Multipath Composition of Sub-6 GHz and mmWave Channels in an Industrial Scenario Using Ray Tracing Simulations

Higo Thaian Pereira da Silva and Ruan Delgado Gomes

Abstract— The integration of fifth-generation networks with Industrial Internet of Things (IIoT) applications is pivotal for fulfilling the technical demands of Industry 4.0, including robust data traffic, minimal latency, and high data throughput. However, deploying these networks requires accurate channel models that capture the unique characteristics of industrial indoor settings. This study addresses this need by presenting a comprehensive characterization of channels at 3.5 GHz, 28 GHz and 73 GHz within an indoor factory (InF) environment through ray tracing simulations. These simulations account for specular reflection, diffraction, and diffuse scattering effects. The analysis encompasses path losses, Rice factor, shadowing, and line-of-sight probability, with a focus on delineating contributions from propagation phenomena.

Keywords— Channel modeling, IIoT applications, mmWave, ray tracing.

I. INTRODUCTION

Industry 4.0, denoting the fourth major advancement in industrial operations, explores the concept of intelligent manufacturing through the supervision and automated management of processes. It enhances efficiency by facilitating predictive capabilities, real-time corrections, and adaptive decision-making, all powered by extensive data processing [1]. Integral to Industry 4.0, the Industrial Internet of Things (IIoT) comprises a vast array of interconnected devices, sensors, and machinery. These components collectively generate rich datasets leveraged for optimizing industrial workflows [2]. However, the effective application of IIoT in Industry 4.0 necessitates high reliability in data traffic, low latency, high throughput, and secure communications between devices.

The fifth generation of communication systems (5G) is regarded as a promising solution to meet the technical requirements of Industry 4.0. According to the International Telecommunication Union (ITU), 5G spans three major application scenarios: enhanced mobile broadband (eMBB), ultra-reliable and low-latency communications (URLLC) and massive machine-type communications (mMTC) [4]. While eMBB applies to user-centric applications, enabling access to multimedia content and services, URLLC and mMTC modes are suited for industrial scenarios, allowing connections among a large number of devices in scenarios that demand high reliability and low latency [3]. Most IIoT services are allocated in the sub-6 GHz band, specifically at 2.6 GHz, 3.4 GHz-3.8 GHz and 4.9 GHz [7]. However, 5G applications extend into the millimeter wave (mmWave) band, typically defined as the frequency range between 30 GHz and 100 GHz. Applications in this high frequency range encounter several challenges, including significant path losses, low diffraction power, high blocking losses, attenuation due to atmospheric molecular absorption, and susceptibility to diffuse scattering. The latter refers to dispersion resulting from surface roughness, which, in high frequency applications, is of a similar order of magnitude to the wavelength [14].

The design, analysis and implementation of IIoT networks is fundamentally dependent on channel models that can capture the specificities of indoor factory (InF) scenarios in multiple frequency range. These environments present unique challenges that differentiate them from traditional indoor settings. InF scenarios are often characterized by a large physical environment, with high ceiling and a prevalence of metallic obstructions such as machinery and racks, leading to significant penetration losses and pronounced specular reflection components [6]. Conversely, the phenomenon of diffraction can mitigate shading in obstructed areas, particularly in applications operating within the sub-6 GHz band. However, in applications operating in the millimeter-wave spectrum, the impact of diffraction on the link is diminished and the diffuse scattering field is significant [8].

In this study, an analysis of communication channels within InF scenarios is performed using ray-tracing simulations. These simulations consider carriers at 3.5 GHz, 28 GHz and 73 GHz, thereby covering both sub-6 GHz and mmWave industrial applications. The shooting-and-bouncing-rays (SBR) method is used in ray tracing, incorporating reflections, diffractions, diffuse scattering, and atmospheric molecular absorption to accurately characterize propagation phenomena. The primary contributions of this work include the characterization of path losses, shadow deviation, Rice factor and line-of-sight probability, along with an analysis of the impact of propagation phenomena on link composition in InF scenarios.

The structure of this paper is as follows: Section II provides a detailed description of the employed ray tracing method, the propagation environment model, and the channel model. Section III presents the numerical results derived from the ray tracing simulations. Finally, Section IV offers the conclusions drawn from this study.

II. RAY TRACING MODELING

Applying the SBR method, the ray tracing algorithm comprises three primary stages: transmission, tracing, and reception [10], [11]. During the transmission stage, multiple rays are emitted along the angular sphere from a designated source point. Achieving a uniform power density and isotropic transmission requires a homogeneous distribution of rays per unit solid angle. The resolution and density of the rays in the simulations are determined by the angle between adjacent rays, which is denoted by the constant $\Delta\theta$. In the tracing stage, the ray lengths progressively increase. At each incremental step, the algorithm checks whether the ray has approached any object. If objects are detected nearby, ray-object interception tests are conducted, in which, if an intersection occurs, the ray is reflected according to Snell's law. These interactions may spawn new ray sources, applied in characterizing the diffraction and diffuse scattering phenomena [13]. Lastly, in the reception stage, virtual spheres are defined around the receiver points. Rays that intercept these reception spheres contribute to the channel impulse response (CIR) of the corresponding link.

One of the results of this work refers to the characterization of the contributions of different propagation phenomena to the channel gain, namely the direct incidence, specular reflection, diffraction, and diffuse scattering. The following equations express the normalized powers of rays associated with each phenomenon, disregarding the radiation patterns of the antennas on the link. Firstly, a line-of-sight (LoS) ray has normalized power described by

$$p_{\text{LoS}} = \left(\frac{\lambda}{4\pi d}\right)^2 \rho_{\text{p}}\rho_{\text{a}}, \quad (1)$$

in which λ is the wavelength, d is the path length and ρ_{p} and ρ_{a} represent the polarization mismatch loss [15] and the frequency-dependent atmospheric molecular absorption attenuation factor, respectively. The latter is calculated following the model outlined in the recommendation ITU-R P.676 and incorporates losses due to dry air and water vapor [16]. In turn, an N_{re}-th order reflection ray has power given by

$$p_{\text{re}} = \left(\frac{\lambda}{4\pi d}\right)^2 \left(\prod_{n=1}^{N_{\text{re}}} \rho_{\text{ds};n}^2 \Gamma_n^2\right) \rho_{\text{p}}\rho_{\text{a}}, \quad (2)$$

in which, in this equation, d represents the total unfolded optical length of the reflected ray and Γ_n represents the n-th reflection loss, calculated based on Fresnel coefficients. If the reflection surface is sufficiently rough[1], the effect of scattering losses in the specular direction, denoted as $\rho_{\text{ds};i}^2$, is considered. This factor is calculated by

$$\rho_{\text{ds};i} = \exp\left\{-\frac{1}{2}\left[\frac{4\pi\sigma_{\text{h}}\cos(\theta_i)}{\lambda}\right]\right\}, \quad (3)$$

in which σ_{h} is the effective roughness of the illuminated surface and θ_i is the incidence angle.

[1]According to the Rayleigh criterion, a surface is classified as electromagnetically rough if $\sigma_{\text{h}} > \lambda/[8\cos(\theta_i)]$ [20].

Following the uniform theory of diffraction (UTD) methodology, an N_{d}-th order diffraction ray has normalized power calculated by

$$p_{\text{d}} = \left(\frac{\lambda}{4\pi\ell_{\text{i}}}\right)^2 \left(\prod_{n=1}^{N_{\text{d}}} A_n^2 D_n^2\right) \rho_{\text{p}}\rho_{\text{a}}, \quad (4)$$

in which ℓ_{i} is the incident length at the first diffracting wedge and A_n and D_n are the spread factor and diffraction loss of the n-th diffracting interaction [19]. Finally, the normalized power of a diffuse scattering ray is expressed as

$$p_{\text{ds}} = \left(\frac{\lambda}{4\pi\ell_{\text{i}}}\right)^2 \left[\frac{A_s^2\cos(\theta_{\text{i}})^2}{\lambda^2\ell_{\text{s}}^2}\zeta_s\right] \rho_{\text{p}}\rho_{\text{a}}, \quad (5)$$

where ℓ_{i} and ℓ_{s} are the lengths of the incidence and scattering paths, respectively; A_s is the illuminated area on the rough surface and ζ is the average scattered power in an arbitrary direction, calculated according to Beckmann-Kirchhoff theory [13], [17].

A. Propagation Environment Model

The ray tracing simulations were conducted within an indoor setting replicating an industrial warehouse, located at the Innovation Hub of the Federal Institute of Paraíba in the city of João Pessoa, Brazil. Considering the wall thickness of 0.2 m, this room has an area A_{env} = 8.3 m×18.35 m and is delimited by concrete and plaster walls. In addition, its structure contains two metal gates, each 3.3 m long, and glass windows. The ceiling height of the room is 3 m. Inside, there are metallic elements that represent industrial machinery equipment. All of these elements have a height of 1.8 m. Fig. 1 presents a detailed description of the dimensions of the propagation environment considered. The complex permittivity of the materials present in the propagation environment was extracted (considering the frequency bands evaluated in this work) applying the methodology described in the ITU-R Recommendation P.2040 [21].

To model the effect of diffuse scattering, the effective roughness of the materials must be characterized. For this, it is assumed that for concrete and plasterboard surfaces, the effective roughnesses are σ_{h} = 0.5 mm and σ_{h} = 0.15 mm, respectively [22], [23]. The metal and glass surfaces are assumed to be smooth ($\sigma_{\text{h}} \approx 0$ mm). In the simulations, the entire environment is subdivided into N_{mr} square microregions, where the reception points are located in their centers at a height h_{rx}, composing a reception grid. Each receiver in this grid is indexed by a pair (i, j).

B. Ray Tracing Channel Modeling

Considering that the receiving point indexed by (i, j) captured $N_{\text{r};i,j}$ rays, its CIR is determined by the superposition expressed by

$$h_{i,j}(\tau) = \sum_{n=1}^{N_{\text{r};i,j}} \sqrt{p_{\text{p};n,i,j}} \exp\left(-j\varphi_{n,i,j}\right) \delta(\tau - \tau_{n,i,j}), \quad (6)$$

in which τ is the delay domain and $p_{\text{p};n,i,j}$, $\varphi_{n,i,j}$ and $\tau_{n,i,j}$ are the normalized power, phase and delay of the n-th received
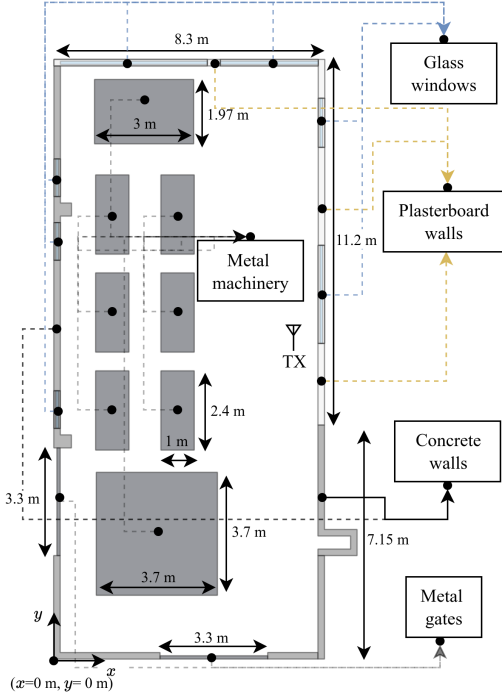
Fig. 1: Description of the propagation environment.

ray, respectively. The term $\mathrm{p} \in \{\mathrm{LoS}, \mathrm{re}, \mathrm{d}, \mathrm{ds}\}$ in $p_{\mathrm{p};n,i,j}$ indicates the physical phenomenon that generated the ray, following the terminology in (1), (2), (4) and (5). Assuming fast phase fluctuations, so that $\varphi_{n,i,j}, \forall n$, can be modeled by mutually independent and uniformly distributed random variables between $[-\pi, \pi]$, it can be demonstrated that the channel power delay profile (PDP) is expressed by

$$P_{i,j}(\tau) \triangleq \mathbb{E}\left[|h_{i,j}(\tau)|^2\right] = \sum_{n=1}^{N_{\mathrm{r};i,j}} p_{\mathrm{p};n,i,j}\delta(\tau - \tau_{n,i,j}), \quad (7)$$

with $\mathbb{E}[\cdot]$ representing the expected value operator. The channel gain, which is denoted as $\beta_{i,j}$ and represents the total multipath power, is calculated by integrating the PDP in the delay domain, resulting in

$$\beta_{i,j} \triangleq \int_{-\infty}^{\infty} P_{i,j}(\tau)d\tau = \sum_{n=1}^{N_{\mathrm{r};i,j}} p_{\mathrm{p};n,i,j}. \quad (8)$$

To analyze the channel gain in terms of its constituent propagation phenomena, $\beta_{i,j}$ is segmented as

$$\beta_{i,j} = \beta_{\mathrm{LoS};i,j} + \beta_{\mathrm{re};i,j} + \beta_{\mathrm{ds};i,j} + \beta_{\mathrm{d};i,j}. \quad (9)$$

In (9), $\beta_{\mathrm{LoS};i,j} = p_{\mathrm{LoS};i,j}$ represents the line-of-sight power (if such conditions exist on the link), while $\beta_{\mathrm{p};i,j}, \mathrm{p} \in \{\mathrm{re}, \mathrm{d}, \mathrm{ds}\}$ denotes the contribution of the remaining effects. These contributions are computed by

$$\beta_{\mathrm{p};i,j} = \sum_{m \in \mathcal{M}_{\mathrm{p}}} p_{\mathrm{p};m,i,j}, \mathrm{p} \in \{\mathrm{re}, \mathrm{d}, \mathrm{ds}\}, \quad (10)$$

in which $\mathcal{M}_{\mathrm{p}}$ represents the set of multipath component indices corresponding to the physical phenomenon identified by

p. Thus, the relative power of each propagation phenomenon within the link composition can be measured by

$$\kappa_{\mathrm{p};i,j} = \frac{\beta_{\mathrm{p};i,j}}{\beta_{i,j}}, \mathrm{p} \in \{\mathrm{LoS}, \mathrm{re}, \mathrm{d}, \mathrm{ds}\}. \quad (11)$$

The distance-dependent average path losses, derived from the channel gain $\beta_{i,j}$, can be parameterized using the close-in free-space (CI) reference model. This model expresses path losses in dB according to [14]

$$\mathrm{PL}_{\mathrm{CI}}(f, d, \eta) = \mathrm{PL}_{\mathrm{FS}}(f, d_0) + 10\eta \log_{10}(d), \quad (12)$$

with f representing the frequency, d denoting the distance between the transmitter and the receiver point, η is the propagation exponent and $\mathrm{PL}_{\mathrm{FS}}(f, d_0)$ is the free-space path loss (expressed in dB) calculated at a reference distance d_0, usually adopted as 1 m [14]. The η parameter is determined by minimizing the mean squared error using channel gain data obtained from simulations. The channel shadowing level, defined as the fluctuation of path losses around the mean curve, is calculated (in dB) as

$$\chi_{i,j} = \mathrm{PL}_{\mathrm{CI}}(f, d_{i,j}, \eta) - 10\log_{10}(\beta_{i,j}), \quad (13)$$

in which $d_{i,j}$ is the distance between the transmitter and the (i, j)-th receiver. The overall shadowing of the channel is quantified by the sample standard deviation of $\chi_{i,j}$, denoted as σ_χ.

Another relevant parameter for channel characterization is the Rice factor, defined as the ratio between the direct sight power and the total scattered power, that is,

$$K_{i,j} = \frac{\beta_{\mathrm{LoS};i,j}}{\beta_{i,j} - \beta_{\mathrm{LoS};i,j}}. \quad (14)$$

To study the dependence of the Rice factor on distance, the following expression is proposed:

$$\bar{K}(d; a_K, b_K) = b_K + 10a_K \log_{10}(d), \quad (15)$$

in which $\bar{K}(d; a_K, b_K)$ is the distance-dependent average Rice factor (expressed in dB) and a_K and b_K are fit parameters. The probability of a given receiver being in line-of-sight (LoS) conditions is often modeled with a distance-dependent expression. In this work, the 3GPP indoor LoS probability model is applied, which is expressed by [9]

$$\mathrm{P}_{\mathrm{LoS}}(d_{2\mathrm{D}}) = \begin{cases} 1, & d_{2\mathrm{D}} \leq d_1, \\ \exp\left(-\frac{d_{2\mathrm{D}}-d_1}{a_{\mathrm{LoS}}}\right), & d_2 \geq d_{2\mathrm{D}} > d_1, \\ \exp\left(-\frac{d_{2\mathrm{D}}-d_2}{b_{\mathrm{LoS}}}\right)\exp\left(-\frac{d_2-d_1}{a_{\mathrm{LoS}}}\right), & d_{2\mathrm{D}} > d_2, \end{cases} \quad (16)$$

with $(a_{\mathrm{LoS}}, b_{\mathrm{LoS}}, d_1, d_2)$ being parameters that best fit the simulation results and $d_{2\mathrm{D}}$ is the 2D distance between transmitter and receiver.

III. NUMERICAL RESULTS

The ray tracing simulations were performed in the InF scenario presented in Section II-A considering a transmitter positioned at coordinates (6.8 m, 17.3 m), as marked in Fig. 1, at a height of $h_{\mathrm{tx}} = 3$ m (transmitter attached to the ceiling of the room). The reception grid contains $N_{\mathrm{mr}} = 28114$

reception points, located at a height of 1.5 m. The channels were analyzed with carriers at 3.5 GHz, 28 GHz and 73 GHz. The ray tracing is performed considering an angular increment between adjacent rays of $\Delta\theta = 0.135°$ and with a maximum of six reflections per optical path. Only first-order diffraction and diffuse scatterings were considered in the simulations. Furthermore, the antennas on the links (transmitting and receiving) are assumed to be vertically polarized. Table I summarizes the specifications of the ray tracing simulations.

TABLE I: Ray tracing simulation specifications.

Parameter	Value
TX position	(6.8 m, 17.3 m)
TX height − h_{tx}	3 m
Number of reception points − N_{mr}	28114
RX height − h_{rx}	1.5 m
Carrier frequency	3.5 GHz, 28 GHz, 73 GHz
Angle resolution − $\Delta\theta$	0.135°
Maximum number of reflections	6
Links polarization	Vertical-Vertical

Table II summarizes the parameters found from the ray tracing simulations. Applying the CI model, the path losses are parameterized for both LoS and Non-LoS (NLoS) links. It is noteworthy that in LoS channels, the propagation exponent remains consistently around 1.32-1.4 across all evaluated frequency carriers. In turn, in obstructed links, this exponent varies from 1.88 (at 3.5 GHz) to 2.0 (at 73 GHz). These relatively low propagation exponent values can be attributed to the waveguide effect induced by indoor environments. Moreover, the dense presence of metallic objects in the InF environment promotes the dispersion of high intensity components, such as low-order reflections; reducing the rate of variation in path losses. The standard deviation of shadowing on LoS links is approximately stable at $\sigma_\chi \approx 1$ dB with respect to frequency. On the other hand, in NLoS channels, this factor has a maximum at $\sigma_\chi = 5.59$ dB for operations at 73 GHz. As expected, channels at 73 GHz generally impose more severe propagation conditions, with higher propagation exponents and shadow deviations. Fig 2 presents the path loss results obtained from the simulation and the corresponding CI models, considering a carrier at 73 GHz.

TABLE II: Channel parameters obtained from ray tracing simulations.

Parameter		Frequency (GHz)		
		3.5	28	73
PLE − η	LoS	1.32	1.32	1.40
	NLoS	1.88	1.90	2.0
SF STD − σ_χ (dB)	LoS	1.00	1.01	1.06
	NLoS	4.91	5.08	5.59
Rice Factor − K	a_K	-1.41	-1.43	-1.58
	b_K (dB)	7.43	7.65	9.10
LoS Probability	d_1 (m)	2.4		
	d_2 (m)	8.8		
	a_{LoS}	8.3		
	b_{LoS}	0.4		
Avg. Relative Powers (dB)	κ_{re}	-1.65	-1.67	-1.88
	κ_d	-33.49	-28.99	-29.50
	κ_{ds}	−	−	-37.52

In turn, the dependence of the Rice factor on distance is characterized by parameters a_K and b_K, as expressed
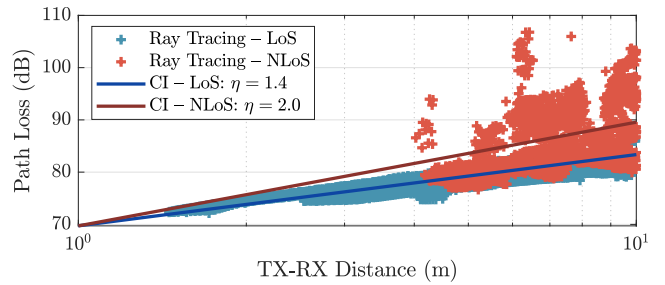

Fig. 2: Path loss results and CI models from ray tracing simulations at 73 GHz.

in (15). Based on the simulation results, the factor a_K, which indicates the rate of decay of the Rice factor with distance, was characterized as -1.41, -1.43 and -1.57 for the carriers at 3.5 GHz, 28 GHz and 73 GHz, respectively. On the other hand, the b_K factor, which indicates the average value of the Rice factor in the vicinity of the receiver, had a maximum value of 9.1 dB at 73 GHz. This is due to the greater relative contribution of the direct incidence component with increasing frequency. Fig. 3a presents the results of the Rice factor and the corresponding model for simulations on 73 GHz channels. According to the simulation results, the LoS probability is parameterized with approximately equal parameters for the three considered carriers. These parameters are $d_1 = 2.4$ m, $d_2 = 8.8$ m, $a_{LoS} = 8.3$ and $b_{LoS} = 0.4$. Fig. 3b presents the simulation results for LoS probability overlaid by the corresponding 3GPP model.
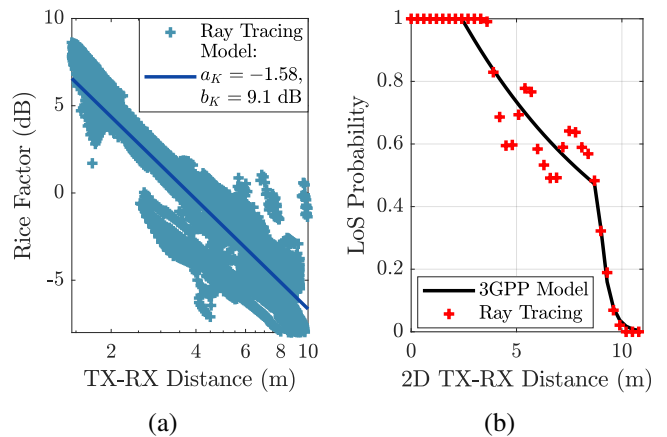

(a)

(b)

Fig. 3: (a) Rice factor results and model from ray tracing simulations at 73 GHz and (b) LoS probability ray tracing results and corresponding 3GPP model.

Table II presents the average values of the relative power parameters κ_{re}, κ_d and κ_{ds}. Examining these values, it becomes evident that specular reflection emerges as the predominant dispersive effect, with its average relative power ranging from -1.88 dB (at 73 GHz) to -1.65 dB (at 3.5 GHz). This dominance can be attributed to two primary factors. Firstly, within indoor settings, the short propagation paths associated with reflections generate components of high intensity. Secondly, the layout of metallic objects within the InF environment generates reflections characterized by high coefficients that approach

unity. It can be seen that the diffraction phenomenon has a low average contribution to the link in both sub-6 GHz and mmWave applications, reaching a minimum average value of -33.49 dB at 3.5 GHz. The diffuse scattering has negligible effects on channels operating at 3.5 GHz and 28 GHz, due to the relatively smooth surfaces (taking into account the effective roughnesses described in Section II-A) compared to the wavelengths in these applications. However, at 73 GHz, where the wavelength is the shortest among those evaluated, the influence of diffuse scattering becomes evident, manifesting itself as an average contribution to the link of -37.52 dB, representing an approximate 8 dB difference compared to diffraction. Fig. 4 presents the empirical cumulative distribution functions (ECDF) of the relative powers of reflection, diffraction, and diffuse scattering.
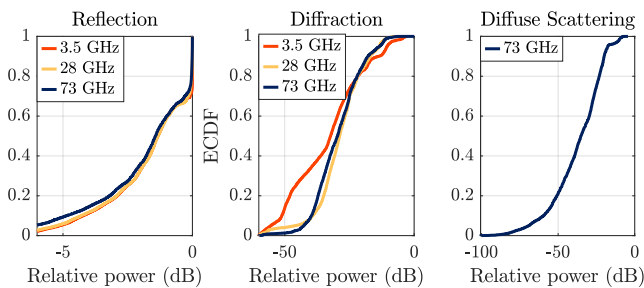

Fig. 4: ECDFs of the relative powers of propagation phenomena for channels at 3.5 GHz, 28 GHz and 73 GHz.

IV. CONCLUSIONS

This study presents channel characterizations at three distinct frequency bands: 3.5 GHz, 28 GHz and 73 GHz, within an indoor factory (InF) environment through ray tracing simulations. The results reveal that, in the evaluated InF scenario, the propagation exponents are diminished due to the waveguide effect, coupled with the significant contribution of high intensity reflected components. A logarithmic decay profile of the Rice factor with distance was also observed, in which, for channels at 73 GHz, the average Rice factor was characterized at 9.1 dB in the vicinity of the transmitter. In the analysis of propagation phenomena, the dominance of specular reflection in the channel composition was observed. Furthermore, at 73 GHz, the effect of diffuse scattering is already comparable to the effect of diffraction.

REFERENCES

[1] T. Ainsworth, J. Brake, P. Gonzalez, D. Toma and A. F. Browne, "A Comprehensive Survey of Industry 4.0, IIoT and Areas of Implementation," SoutheastCon 2021, Atlanta, GA, USA, 2021, pp. 1-6, doi: 10.1109/SoutheastCon45413.2021.9401860

[2] M. Vaezi et al., "Cellular, Wide-Area, and Non-Terrestrial IoT: A Survey on 5G Advances and the Road Toward 6G," in *IEEE Communications Surveys & Tutorials*, vol. 24, no. 2, pp. 1117-1174, Secondquarter 2022, doi: 10.1109/COMST.2022.3151028.

[3] B. S. Khan, S. Jangsher, A. Ahmed and A. Al-Dweik, "URLLC and eMBB in 5G Industrial IoT: A Survey," in *IEEE Open Journal of the Communications Society*, vol. 3, pp. 1134-1163, 2022, doi: 10.1109/OJ-COMS.

[4] M. Shafi et al., "5G: A Tutorial Overview of Standards, Trials, Challenges, Deployment, and Practice," in *IEEE Journal on Selected Areas in Communications*, vol. 35, no. 6, pp. 1201-1221, June 2017, doi: 10.1109/JSAC.2017.2692307.

[5] M. R. Akdeniz et al., "Millimeter Wave Channel Modeling and Cellular Capacity Evaluation," in *IEEE Journal on Selected Areas in Communications*, vol. 32, no. 6, pp. 1164-1179, June 2014, doi: 10.1109/JSAC.2014.2328154.

[6] T. Jiang et al., "3GPP Standardized 5G Channel Model for IIoT Scenarios: A Survey," in *IEEE Internet of Things Journal*, vol. 8, no. 11, pp. 8799-8815, 1 June1, 2021, doi: 10.1109/JIOT.2020.3048992.

[7] Huawei and HiSilicon, Survey of Frequency Band of Interest for Industrial IoT, document R1-1813671, 3GPP, Sophia Antipolis, France, Nov. 2018. [Online]. Available: https://www.3gpp.org/dynareport?code=TDocExMtg–R1-95–18807.htm

[8] G. R. Maccartney, T. S. Rappaport, S. Sun and S. Deng, "Indoor Office Wideband Millimeter-Wave Propagation Measurements and Channel Models at 28 and 73 GHz for Ultra-Dense 5G Wireless Networks," in *IEEE Access*, vol. 3, pp. 2388-2424, 2015, doi: 10.1109/ACCESS.2015.2486778.

[9] "Study on channel model for frequencies from 0.5 to 100 GHz, V15.0.0," 3GPP, Sophia Antipolis, France, Rep. TR 38.901, Mar. 2024. [Online]. Available: https://www.3gpp.org/ftp/Specs/archive/38_series/38.901/

[10] Z. Yun and M. F. Iskander, "Ray Tracing for Radio Propagation Modeling: Principles and Applications," in *IEEE Access*, vol. 3, pp. 1089-1100, 2015, doi: 10.1109/ACCESS.2015.2453991.

[11] T. Imai, "A Survey of Efficient Ray-Tracing Techniques for Mobile Radio Propagation Analysis," *IEICE Trans. Commun.*, vol. 100-B, no. 5, pp. 666–679, May 2017.

[12] H. T. P. Da Silva, M. S. De Alencar, W. J. Lira Queiroz and H. S. Silva, "Coverage Probability Analysis of a RIS-Assisted THz Indoor System Based on Ray Tracing Simulations," *2023 IEEE Latin-American Conference on Communications (LATINCOM)*, Panama City, Panama, 2023, pp. 1-6, doi: 10.1109/LATINCOM59467.2023.10361895.

[13] H. T. P. da Silva, H. S. Silva, M. S. Alencar, W. J. L. Queiroz and U. S. Dias, "Characterization of Large-Scale Parameters in Indoor THz Channels Applying the Ray Tracing Method," *2022 Workshop on Communication Networks and Power Systems (WCNPS)*, Fortaleza, Brazil, 2022, pp. 1-6, doi: 10.1109/WCNPS56355.2022.9969765. Recommendation ITU-R P.676-13: Attenuation by Atmospheric Gases and Related Effects," ITU, Tech. Rep. P.676-13, Aug. 2022.

[14] T. S. Rappaport, Y. Xing, G. R. MacCartney, A. F. Molisch, E. Mellios and J. Zhang, "Overview of Millimeter Wave Communications for Fifth-Generation (5G) Wireless Networks—With a Focus on Propagation Models," in *IEEE Transactions on Antennas and Propagation*, vol. 65, no. 12, pp. 6213-6230, Dec. 2017, doi: 10.1109/TAP.2017.2734243.

[15] C. A. Balanis, *Antenna Theory-Analysis and Design*, 3rd ed. Hoboken, NJ, USA: Wiley, 2005.

[16] Recommendation ITU-R P.676-13: Attenuation by Atmospheric Gases and Related Effects, document P.676-13, ITU-R, Aug. 2022.

[17] F. Sheikh, Y. Gao and T. Kaiser, "A Study of Diffuse Scattering in Massive MIMO Channels at Terahertz Frequencies," in *IEEE Transactions on Antennas and Propagation*, vol. 68, no. 2, pp. 997-1008, Feb. 2020, doi: 10.1109/TAP.2019.2944536.

[18] R. J. Luebbers, "A heuristic UTD slope diffraction coefficient for rough lossy wedges," in *IEEE Transactions on Antennas and Propagation*, vol. 37, no. 2, pp. 206-211, Feb. 1989, doi: 10.1109/8.18707.

[19] G. Carluccio, F. Puggelli and M. Albani, "A UTD Triple Diffraction Coefficient for Straight Wedges in Arbitrary Configuration," in *IEEE Transactions on Antennas and Propagation*, vol. 60, no. 12, pp. 5809-5817, Dec. 2012, doi: 10.1109/TAP.2012.2209623.

[20] A. Ishimaru, "Wave propagation and scattering in random media and rough surfaces," in *Proceedings of the IEEE*, vol. 79, no. 10, pp. 1359-1366, Oct. 1991, doi: 10.1109/5.104210.

[21] Recommendation ITU-R P.2040-3: Effects of Building Materials and Structures on Radiowave Propagation Above About 100 MHz, document P.676-13, ITU-R, Aug. 2023.

[22] R. Piesiewicz, C. Jansen, D. Mittleman, T. Kleine-Ostmann, M. Koch and T. Kurner, "Scattering Analysis for the Modeling of THz Communication Systems," in *IEEE Transactions on Antennas and Propagation*, vol. 55, no. 11, pp. 3002-3009, Nov. 2007, doi: 10.1109/TAP.2007.908559.

[23] Pedro M.D. Santos and Eduardo N.B.S. Júlio, "A State-of-the-Art Review on Roughness Quantification Methods for Concrete Surfaces," in *Construction and Building Materials*, vol. 38, pp. 912-923, 2013.